

Systems Involving Hydrogenated and Fluorinated Chains: Volumetric Properties of Perfluoroalkanes and Perfluoroalkylalkane Surfactants

Pedro Morgado,[†] J. Ben Lewis,[‡] Carlos M. C. Laginhas,[§] Luís F. G. Martins,[§] Clare McCabe,[‡] Felipe J. Blas,^{||} and Eduardo J. M. Filipe^{*,†}

[†]Centro de Química Estrutural, Instituto Superior Técnico, Universidade Técnica de Lisboa, 1049-001 Lisboa, Portugal

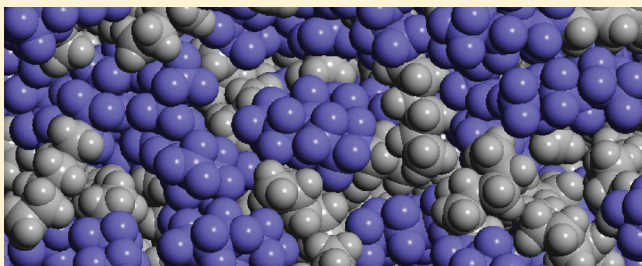
[‡]Department of Chemical and Biomolecular Engineering and Department of Chemistry, Vanderbilt University, Nashville, Tennessee 37235, United States

[§]Centro de Química de Évora, Universidade de Évora, Rua Romão Ramalho, 59, 7000-671 Évora, Portugal

^{||}Departamento de Física Aplicada, Facultad de Ciencias Experimentales, Universidad de Huelva, 21071 Huelva, Spain

 Supporting Information

ABSTRACT: As part of a combined experimental and theoretical study of the thermodynamic properties of perfluoroalkylalkanes (PFAAs), the liquid density of perfluorobutylpentane (F4H5), perfluorobutylhexane (F4H6), and perfluorobutyl-octane (F4H8) was measured as a function of temperature from 278.15 to 353.15 K and from atmospheric pressure to 70 MPa. The liquid densities of *n*-perfluoropentane, *n*-perfluorohexane, *n*-perfluorooctane, and *n*-perfluorononane were also measured at room pressure over the same temperature range. The PVT behavior of the PFAAs was also studied using the SAFT-VR equation of state. The PFAA molecules were modeled as heterosegmented diblock chains, using different parameters for the alkyl and perfluoroalkyl segments, that were developed in earlier work. Through this simple approach, we are able to predict the thermodynamic behavior of the perfluoroalkylalkanes, without fitting to any experimental data for the systems being studied. Molecular dynamics simulations have also been performed and used to calculate the densities of the perfluoroalkylalkanes studied.



1. INTRODUCTION

It is well-known that binary mixtures of alkanes and perfluoroalkanes are highly nonideal systems, in spite of the apparent similarity of the components. These mixtures exhibit large regions of liquid–liquid immiscibility, large positive deviations from Raoult's law, and large positive excess properties (such as the excess enthalpy and volume), a clear indication of weak unlike interactions.

Since the late 1940s, the potential application of perfluoroalkanes as refrigerant fluids has motivated their study. In recent years, however, these substances have become key fluids in a wide range of fields due to their chemical inertness, biocompatibility, and peculiar physical properties,^{1,2} for example, from medical applications, where they find use as oxygen carriers in blood substitute formulations^{3,4} or as fluids in eye surgery, to technological applications as solvents for biphasic synthesis, fire extinguishers, or lubricants.^{5,6} As a result, considerable work has been carried out on the theoretical and computational modeling of *n*-alkane + *n*-perfluoroalkane mixtures^{7–17} to try and understand the nature of the unlike interaction.^{8,9,17} However, apart from repeatedly recognizing the need to account for large deviations to the Lorentz–Berthelot combining rules when estimating the unlike or cross intermolecular potential parameters, all these studies have failed to give a satisfactory explanation for the unusually weak hydrocarbon–fluorocarbon interaction.

Structurally, the substitution of hydrogens for the larger and heavier fluorine atoms results in a larger cross-sectional area for fluorinated chains¹⁸ (0.283 nm² compared to 0.185 nm²) and consequently higher densities and molar volumes for *n*-perfluoroalkanes when compared with *n*-alkanes of the same number of carbon atoms (Figure 1). These large differences in molar volume have other, subtler, consequences. For example, at 25 °C, the molar volume of *n*-hexane is 131.6 cm³ mol⁻¹, and that of *n*-perfluorohexane is almost 54% higher, 202.4 cm³ mol⁻¹. As a result, an equimolar mixture of (*n*-hexane + *n*-perfluorohexane) will have a volume fraction of *n*-perfluorohexane of 0.61, assuming ideality. Consequently, a probe immersed in such a mixture would “experience” a much more fluorinated environment than expected from its equimolar composition.

The changes in volume that occur when mixing hydrogenated and fluorinated compounds are impressive and also deserve closer attention. For example, we have recently reported partial molar volumes at infinite dilution for a series of *n*-perfluoroalkanes in *n*-octane,^{19,20} and found that when a molecule of *n*-perfluorohexane is immersed in *n*-octane, at infinite dilution, its molar volume increases from 202.4 to 229.3 cm³ mol⁻¹, i.e., 13%.

Received: August 7, 2011

Revised: September 20, 2011

Published: September 27, 2011

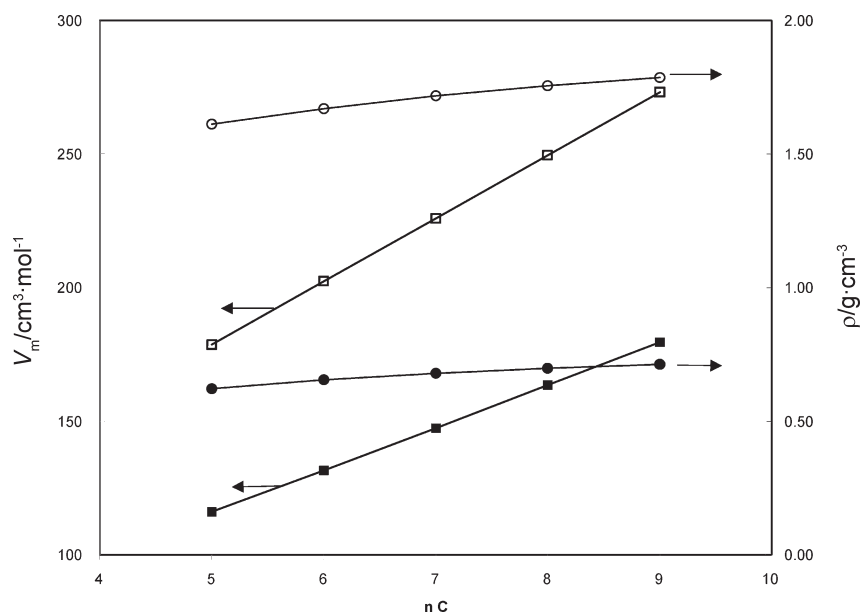


Figure 1. Densities and molar volumes of *n*-alkanes and *n*-perfluoroalkanes at 298.15 K, as a function of number of carbon atoms.

Literally, a layer of empty space is created around the *n*-perfluorohexane molecule. The effect is even more pronounced when *n*-alkanes are dissolved in *n*-perfluoroalkanes: their molar volumes increase by 20%!²¹

Another important difference between fluorinated and hydrogenated chains is conformational. For the *n*-alkanes, the value of the dihedral angle at the energy minimum of a “trans” C–C bond is exactly 180°, so that the chains tend to be in their all-trans planar form. For the *n*-perfluoroalkanes, the dihedral angle at minimum energy is not exactly 180°, and as a consequence, perfluorinated chains display a helical conformation and rigidity, which contrasts with the flexible character of hydrogenated chains.²² It is believed that one of the consequences of chain stiffness in liquid fluorocarbons is less efficient molecular packing and the existence of “holes” in the liquid. This can explain (at least in part) the enhanced solubility of simple gases (e.g., oxygen, nitrogen, etc.) in liquid perfluoroalkanes.

In summary, considerable changes in volume occur when hydrogenated chains are mixed with fluorinated chains. Furthermore, it is clear that an accurate description and interpretation of such changes should provide important information on the nature of the cross interaction between these different functional groups.

Perfluoroalkylalkanes (PFAAs) are diblock compounds made up of alkyl and perfluoroalkyl segments covalently bonded to form a single chain. They can be pictured as chemical mixtures of two mutually phobic segments that in most cases would otherwise phase separate. Interesting volumetric properties can, thus, be expected for these liquids. Additionally, these molecules display the “dual character” of amphiphilic molecules and the physics of orientational ordering of smectogenic liquid crystals. Accordingly, aggregation in solvents selective for one of the blocks^{23,24} and smectic liquid crystalline phases have been reported for PFAAs.^{25–27} It should be kept in mind, however, that unlike common hydrophilic/hydrophobic amphiphiles in which one of the driving forces for organization is the strong interaction between polar or ionic groups, in PFAA, the origin of the mutual segregation between alkyl and perfluoroalkyl groups,

and therefore organization, rests on the weakness of the cross interaction.

This work is part of an ongoing project aiming at a detailed thermophysical characterization of liquid PFAAs. In particular, we have measured a number of properties of the pure liquids (such as liquid densities, vapor pressures, viscosities, surface tensions, and heat capacities) and mixtures (partial molar volumes at infinite dilution, water solubilities, interfacial tensions) and tried to interpret the results using equivalent information from the corresponding alkanes, perfluoroalkanes, and their mixtures. This strategy will ultimately clarify the effects of chemically linking the hydrogenated and perfluorinated segments and how this affects the properties of the new pure liquid and induces organization. Additionally, the results have been theoretically modeled with the SAFT-VR equation and PFAAs studied by computer simulation.

In recent papers,^{19,28} we reported liquid densities as a function of temperature and pressure and partial molar volumes at infinite dilution for two PFAAs (F6H6 and F6H8). In this work we have extended the study to an additional three PFAAs: perfluorobutylpentane (F4H5), perfluorobutylhexane (F4H6), and perfluorobutyloctane (F4H8), for which partial molar volumes at infinite dilution in *n*-octane have also been recently reported.²⁰ Liquid densities have been measured, at room pressure, as a function of temperature from 278.15 to 353.15 K and at 5 K intervals and from atmospheric pressure to 70 MPa. The liquid densities of *n*-perfluoropentane (F5), *n*-perfluorohexane (F6), *n*-perfluorooctane (F8), and *n*-perfluorononane (F9) were also measured at room pressure over the same temperature range. The SAFT-VR equation of state^{29–31} has been used to model the PFAAs as diblock chains, using parameters for the alkyl and perfluoroalkyl segments developed in an earlier work.²⁸ Through this simple approach, we are able to predict the thermodynamic behavior of the PFAAs studied, without fitting to any experimental data for the systems being studied. Additionally, the densities of the PFAAs as a function of temperature and pressure have been predicted by molecular dynamics simulation using an all-atom force field.

2. EXPERIMENTAL SECTION

The perfluoroalkylalkane liquids (F4H5, F4H6, and F4H8) used were ultrapurified chemicals obtained from Fluoron GMBH with a claimed purity of 100%. ^{19}F and ^1H NMR spectra of these compounds were taken in a 500 MHz Bruker spectrometer, and only very small unexpected peaks were found which, when integrated, were smaller than 1%. Hence, these compounds were used without further purification. Perfluoropentane and perfluorononane were obtained from Apollo Scientific, with 97% (85% *n*-isomer) and 99% purity, respectively; perfluorohexane (99%) and perfluorooctane (98%) were sourced from Aldrich. All were used as received.

The density measurements at ambient pressure were made in an Anton Paar DMA 5000 vibrating-tube densimeter. The instrument was calibrated with water (distilled, deionized in a Milli-Q 185 Plus water purification system and freshly boiled) and air at 20.000 °C, taking into account atmospheric pressure. The densimeter has an internal temperature control system that is stable at $T \pm 0.001$ K. The calibration was checked with water over the whole range of operating temperatures, and the maximum deviation from literature values was found to be less than 2×10^{-5} g cm $^{-3}$. The cleanliness of the measurement cell was verified at the beginning of each series of measurements by checking the measured density of air.

The densities at high pressure were measured in an Anton Paar DMA HP external cell, connected to the DMA 5000 densimeter. As in the DMA 5000, the temperature control is internal and stable to $T \pm 0.001$ K; the cell was connected to a high-pressure generator and to a Setra 280E pressure transducer, which has an accuracy of 0.08 MPa. The densimeter was calibrated in vacuum over the whole range of measurement temperatures and with water, toluene, and dichloromethane in the whole range of temperature and pressure, giving a total of 737 calibration points; the average of the absolute residuals of the overall fit in relation to the literature data^{32–34} for the calibrating fluids was 3×10^{-5} g cm $^{-3}$, and the individual deviations were always smaller than 2×10^{-4} g cm $^{-3}$.

3. MOLECULAR MODEL AND THEORY

In the SAFT-VR approach, molecules are modeled as chains of tangentially bonded hard-spherical segments that interact through an attractive potential of variable range, typically a square well (SW) potential, viz.

$$U_{ij}(r) = \begin{cases} +\infty & \text{if } r < \sigma_{ij} \\ -\varepsilon_{ij} & \text{if } \sigma_{ij} \leq r < \lambda_{ij}\sigma_{ij} \\ 0 & \text{if } r \geq \lambda_{ij}\sigma_{ij} \end{cases} \quad (1)$$

where σ_{ij} is the diameter of the interaction, λ_{ij} the range, and ε_{ij} the depth of the SW potential. The SAFT-VR approach has been used to successfully model the thermodynamics and phase behavior of a wide range of fluids, including alkanes, perfluoroalkanes, and their binary mixtures.^{14,35,36} Recently the SAFT-VR approach was extended to model chain fluids composed of dissimilar segments, forming a heteronuclear rather than a homonuclear chain as in the original SAFT-VR approach and used to make predictions for the phase behavior of PFAAs and their mixtures with alkanes and perfluoroalkanes,^{28,30,37} as well as other fluids through a group contribution like approach.^{31,38–40}

Table 1. Optimized SAFT-VR Parameters for the Molecules and Molecular Segments Studied

segment	m	λ	σ , Å	ε/k , K
C ₅ H ₁₁ –	1.998	1.505	3.931	265.0
C ₆ H ₁₃ –	2.332	1.552	3.920	250.4
C ₈ H ₁₇ –	2.998	1.574	3.945	250.3
C ₄ F ₉ –	1.795	1.406	4.462	283.3

Using the heterobased SAFT-VR approach, the parameters describing the alkyl and perfluoroalkyl segments of each perfluoroalkylalkane molecule are reported in Table 1 and discussed further in the Results section. The inter- and intramolecular cross interactions between segments were obtained from the modified Lorentz–Berthelot combining rules⁸

$$\sigma_{ij} = \frac{\sigma_{ii} + \sigma_{jj}}{2} \quad (2)$$

$$\varepsilon_{ij} = \xi_{ij} \sqrt{\varepsilon_{ii}\varepsilon_{jj}} \quad (3)$$

$$\lambda_{ij} = \gamma_{ij} \frac{\lambda_{ii}\sigma_{ii} + \lambda_{jj}\sigma_{jj}}{\sigma_{ii} + \sigma_{jj}} \quad (4)$$

The general form of the Helmholtz energy A within the SAFT framework is given by

$$\frac{A}{NkT} = \frac{A^{\text{ideal}}}{NkT} + \frac{A^{\text{mono}}}{NkT} + \frac{A^{\text{chain}}}{NkT} + \frac{A^{\text{assoc}}}{NkT} \quad (5)$$

We will briefly present each contribution in turn for a nonassociating fluid of diblock-heteronuclear chain molecules and direct the reader to the original references for full details of the hetero-SAFT-VR approach.^{41,29}

The ideal contribution to the Helmholtz energy is expressed as

$$\frac{A^{\text{ideal}}}{NkT} = \ln(\rho\Lambda^3) - 1 \quad (6)$$

where N is the total number of molecules, k Boltzmann's constant, ρ the number density of chain molecules, and Λ the thermal de Broglie wavelength.

The monomer Helmholtz energy is given by

$$\frac{A^{\text{mono}}}{NkT} = m \frac{A^{\text{M}}}{N_s kT} = m a^{\text{M}} \quad (7)$$

where N_s is the total number of segments, determined from the product of the total number of molecules N and the number of segments per molecule m . a^{M} is the Helmholtz energy per monomer segment and is approximated by a second-order high-temperature expansion using Barker and Henderson perturbation theory for mixtures,⁴² viz.

$$a^{\text{M}} = a^{\text{HS}} + \beta a_1 + \beta^2 a_2 \quad (8)$$

where $\beta = 1/kT$; a^{HS} is the Helmholtz energy of the hard sphere reference fluid; and a_1 and a_2 are the first and second perturbation terms, respectively. a^{HS} is determined from the expression of Boublik⁴³ and Mansoori et al.⁴⁴ for multicomponent hard sphere

Table 2. Experimental Densities (kg/m³) at Room Pressure, As a Function of Temperature, For the Studied Substances

T/K	F5	F6	F8	F9	F4H5	F4H6	F4H8
273.15	1691.136	—	—	—	—	—	—
278.15	1675.521	1728.598	1806.278	—	1319.732	1288.097	1236.306
283.15	1659.678	1714.274	1793.773	1823.265	1311.591	1280.509	1229.510
288.15	1643.569	1699.762	1781.182	1811.355	1303.419	1272.913	1222.719
293.15	1627.182	1685.093	1768.496	1799.074	1295.205	1265.271	1215.899
298.15	—	1670.204	1755.710	1786.992	1286.961	1257.626	1209.078
303.15	—	1655.126	1742.819	1774.577	1278.644	1249.902	1202.221
308.15	—	1639.795	1729.817	1762.358	1270.328	1242.207	1195.395
313.15	—	1624.241	1716.678	1749.718	1261.909	1234.410	1188.486
318.15	—	1608.574	1703.415	1737.310	1253.493	1226.631	1181.614
323.15	—	1592.415	1690.000	1724.448	1244.958	1218.756	1174.665
328.15	—	—	1676.434	1711.814	1236.408	1210.873	1167.729
333.15	—	—	1662.695	1698.700	1227.757	1202.894	1160.729
338.15	—	—	1648.789	1685.806	1219.052	1194.907	1153.726
343.15	—	—	1634.681	1672.403	1210.242	1186.822	1146.657
348.15	—	—	1620.442	1659.219	1201.379	1178.701	1139.578
353.15	—	—	1605.894	1645.677	1192.404	1170.494	1132.442

Table 3. Coefficients Obtained by Fitting the Room Pressure Density Data As a Function of Temperature to Equation 12 for All Compounds Studied

	a_0	a_1	a_2	a_3
F5	2150.349	-26.862	-51.7143	-
F6	2667.943	-528.269	118.118	-17.8353
F8	2669.416	-470.121	93.0836	-12.8093
F9	2577.846	-358.068	55.3886	-8.13809
F4H5	1859.697	-271.007	43.9794	-5.87410
F4H6	1778.493	-236.082	34.0669	-4.52142
F4H8	1678.952	-208.635	27.2040	-3.38282

systems, while a_1 is obtained from the mean-value theorem and a_2 through the local compressibility approximation, as proposed by Gil-Villegas et al.⁴⁵

$$K^{\text{HS}} = \frac{\xi_0(1 - \xi_3)^4}{\xi_0(1 - \xi_3)^2 + 6\xi_1\xi_2(1 - \xi_3) + 9\xi_2^3} \quad (9)$$

Finally, the contribution due to chain formation from the monomer segments is given in terms of the background correlation function y_{ij}^{SW}

$$\frac{A^{\text{chain}}}{NkT} = - \sum_{ij \text{ bonds}} \ln y_{ij}^{\text{SW}}(\sigma_{ij}) = \exp(-\beta\varepsilon_{ij})g_{ij}^{\text{SW}}(\sigma_{ij}) \quad (10)$$

where the sum is over all bonds in the chain molecule. For the PFAAs studied in this work, eq 10 becomes

$$\frac{A^{\text{chain}}}{NkT} = -(m_1 - 1)\ln y_{11}^{\text{SW}}(\sigma_{11}) - (m_2 - 1)\ln y_{22}^{\text{SW}}(\sigma_{22}) - \ln y_{12}^{\text{SW}}(\sigma_{12}) \quad (11)$$

where component one refers to the alkyl segments and two to the perfluoroalkyl segments of the PFAA. The radial distribution function for the square well monomers $g_{ij}^{\text{SW}}(\sigma_{ij})$ is approximated

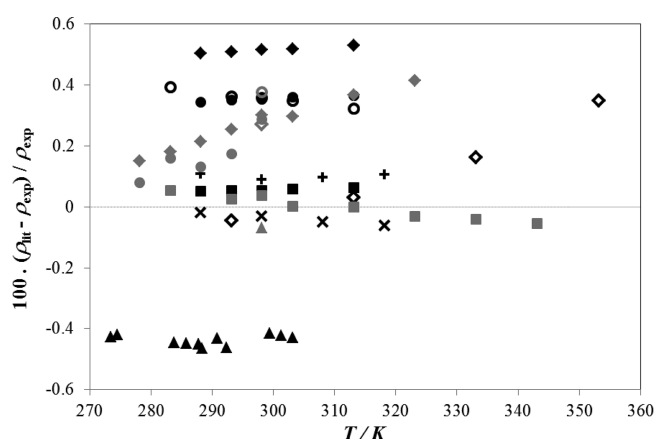


Figure 2. Comparison between the density of liquid *n*-perfluoroalkanes obtained in this work and data from the literature. Gray triangle, F5 from Lepori et al.;²¹ black triangle, F5 from Burger et al.;⁶⁰ black circle, F6 from Dias et al.;⁶¹ black x, F6 from Dunlap et al.⁶² (air saturated liquid); black plus, F6 from Dunlap et al.⁶² (degassed liquid); open circle with black border, F6 from Piñeiro et al.;⁵³ open circle with gray border, F6 from Kennan et al.;⁶³ gray circle, F6 from Lepori et al.;²¹ black diamond, F8 from Dias et al.;⁶⁴ gray diamond, F8 from Kennan et al.;⁶³ open diamond with gray outline, F8 from Lepori et al.;²¹ open diamond with black outline, F8 from Mustafaev et al.;⁶⁵ black square, F9 from Dias et al.;⁶¹ gray square, Piñeiro et al.⁵³

by a first-order high-temperature perturbation expansion, again following the work of Gil-Villegas et al.⁴⁵

4. SIMULATION DETAILS

The optimized potentials for liquid simulations all-atom (OPLS-AA) force field⁴⁶ with the extension to perfluoroalkanes by Watkins and Jorgensen⁴⁷ has been used to describe the PFAA molecules. In the OPLS-AA force field a Lennard-Jones potential describes the intermolecular interactions and the intramolecular interactions between sites separated by three or more bonds.

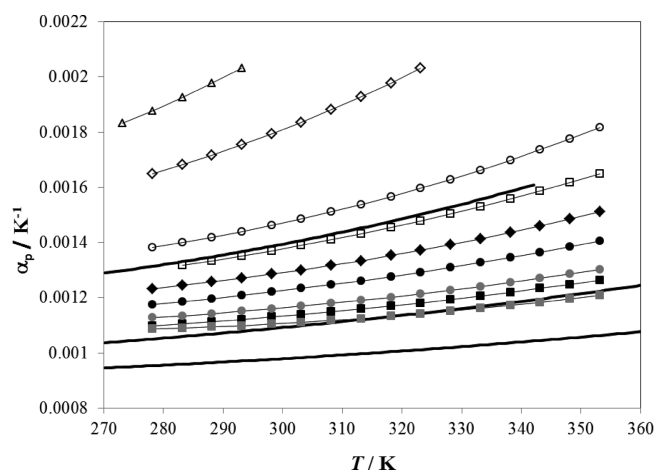


Figure 3. Isobaric thermal expansion coefficients at atmospheric pressure as a function of temperature for the studied substances (F6H6 and F6H8 from previous work²⁸) and selected *n*-alkanes (*n*-hexane, *n*-nonane, and *n*-dodecane, as solid lines). F5, Δ ; F6, \diamond ; F8, \circ ; F9, \square ; F4H5, \blacklozenge ; F4H6, \bullet ; F6H6, gray circle; F4H8, \blacksquare ; F6H8, gray box. The results for the *n*-alkanes were calculated from the density correlations of Cibulka.⁵⁵

Simple geometric combining rules were used to determine the cross or unlike interactions. Bond stretching and bond angle bending are described by harmonic potentials, and torsional motion characterizing the preferred orientational and rotational barriers around all nonterminal bonds is described through the potentials of Jorgensen and Pádua.⁴⁸

All simulations were performed with 243 molecules in the isobaric–isothermal (NpT) ensemble using the Nosé–Hoover thermostat and barostat in the LAMMPS molecular dynamics code.⁴⁹ The particle–particle particle–mesh (PPPM) algorithm with a precision of 1.0×10^{-6} was used to describe the long-range electrostatic interactions and a spherical potential cut off of 12 Å used for the van der Waals interactions. All simulations were run using a time step of 1.0 fs for 2 ns, with the last 1 ns of data used to determine the density using block averaging.⁵⁰

5. RESULTS

The experimental densities as a function of temperature (at atmospheric pressure) are presented in Table 2. The results have been correlated with a simple polynomial of the form

$$d/\text{kg m}^{-3} = \sum_{i=0}^n a_i(T/100 \text{ K})^i \quad (12)$$

where d is the density and T the absolute temperature. The obtained coefficients allow the reproduction of the experimental values within the reproducibility of the measurements and are collected in Table 3.

In the case of the *n*-perfluoroalkanes, the experimental results can be compared with values already available in the literature, although over a smaller temperature range as shown in Figure 2. As can be seen from the figure, our results compare favorably with the literature data, with differences that never exceed 0.5% and that are most probably due to the different sources of the perfluoroalkane samples. The exceptions are the results from Haszeldine⁵¹ and Stiles,⁵² which present deviations from ours

Table 4. Coefficients Obtained by Fitting the Density Data as a Function of Temperature and Pressure to Equation 15 for the Three PFAAs Studied, Along with the Standard Deviation of the Fitting

	F4H5	F4H6	F4H8
C	8.36992×10^{-2}	8.36390×10^{-2}	8.34046×10^{-2}
B_0/MPa	320.675	329.632	345.294
$B_1/\text{MPa K}^{-1}$	-1.32734	-1.34419	-1.37807
$B_2/\text{MPa K}^{-2}$	1.43613×10^{-3}	1.44204×10^{-3}	1.46350×10^{-3}
$\rho_{00}/\text{kg m}^{-3}$	1720.207	1673.601	1601.261
$\rho_{01}/\text{kg m}^{-3} \text{ K}^{-1}$	-1.22726	-1.23374	-1.24882
$\rho_{02}/\text{kg m}^{-3} \text{ K}^{-2}$	-7.59985×10^{-4}	-5.42706×10^{-4}	-2.26929×10^{-4}
$\sigma/\text{kg cm}^{-3}$	7.2×10^{-2}	5.9×10^{-2}	4.2×10^{-2}

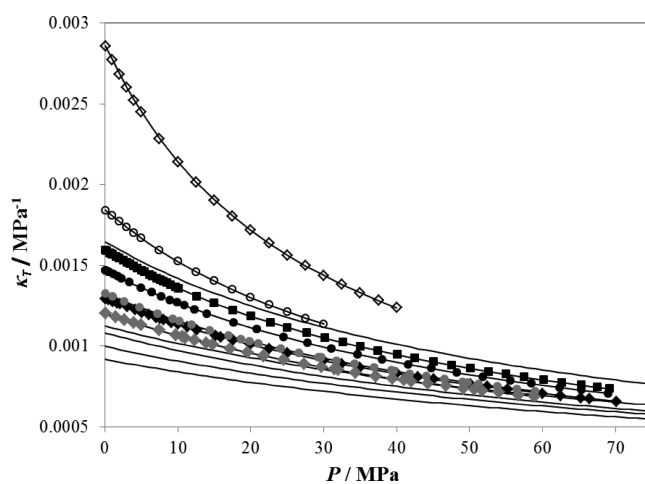


Figure 4. Isothermal compressibility coefficients at 298.15 K as a function of pressure for the studied PFAA, along with the results for selected *n*-alkanes (*n*-hexane, *n*-nonane, *n*-decane, *n*-dodecane, and *n*-tetradecane, as solid lines) and *n*-perfluoroalkanes. F6, \diamond ; F9, \circ ; F4H5, \blacksquare ; F4H6, \bullet ; F6H6, gray circle; F4H8, \blacklozenge ; F6H8, gray diamond. The results for the *n*-alkanes were calculated from the density correlations of Cibulka.⁵⁵

not exceeding 1.5 and 0.75%, respectively, and are not included in the figure for simplicity.

From the dependence of density with temperature, the isobaric thermal expansion coefficient

$$\alpha_p = -\frac{1}{\rho} \left(\frac{\partial \rho}{\partial T} \right)_p \quad (13)$$

can be calculated and was done by analytical differentiation of eq 12. α_p coefficients for all the studied substances are recorded in Figure 3 along with data for F6H6 and F6H8, which were calculated from data obtained in previous work,²⁸ and data for selected *n*-alkanes for comparison.

Liquid densities for F4H5, F4H6, and F4H8 were also determined as a function of pressure. Isothermal curves were measured at 5 K intervals between 278.15 and 353.15 K, from atmospheric pressure to 70 MPa; at least 30 points were taken along each isotherm, for a total of almost 600 data points for each substance. These values were fitted with the widely used

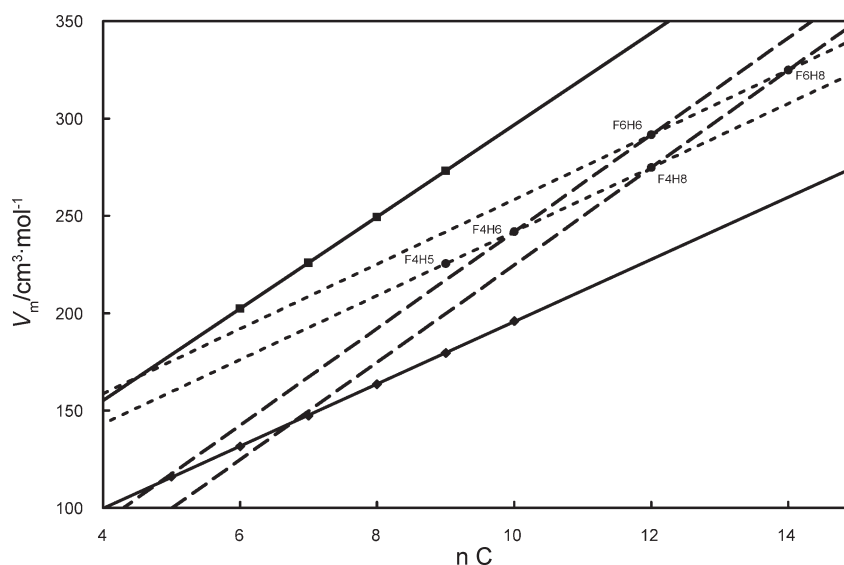


Figure 5. Molar volumes at 298.15 K and atmospheric pressure for all the PFAA and *n*-perfluoroalkanes studied as a function of number of carbon atoms. Molar volumes of *n*-alkanes at the same conditions are also included for comparison.

modified Tait equation

$$\rho(p, T) = \rho_0(T) / \left(1 - C \ln \left(\frac{B(T) + p}{B(T) + p_0} \right) \right) \quad (14)$$

where $\rho_0(T)$, C , and $B(T)$ are the fitting parameters. $\rho_0(T)$ stands for the density at the reference pressure $p_0 = 0.101325$ MPa and is given by $\rho_0(T) = \sum_{i=0}^2 \rho_{0i} T^i$. C is temperature independent, and $B(T)$ is given by $B(T) = \sum_{i=0}^2 B_i T^i$. The fitting coefficients for the three compounds are presented in Table 4, along with the standard deviation of the fit, calculated as

$$\sigma = \sqrt{\frac{\sum_{i=1}^n (\rho_{\text{exp}} - \rho_{\text{calc}})^2}{n}} \quad (15)$$

where n is the number of experimental points. The full set of experimental data is too large to be conveniently presented in the main body of this paper and so is provided as Supporting Information.

From the dependence of the density with pressure, the isothermal compressibility coefficient

$$\kappa_T = \frac{1}{\rho} \left(\frac{\partial \rho}{\partial p} \right)_T \quad (16)$$

can be calculated. In this case, analytical differentiation of the Tait eq 14 is the most straightforward and accepted way to obtain κ_T .⁸ In Figure 4 the compressibilities at 298.15 K for the studied PFAAs are represented, together with those of F6H6 and F6H8 from previous work,²⁸ two perfluoroalkanes from the work of Piñeiro et al.,⁵³ and data for some selected alkanes, calculated from the correlations of Cibulka.⁵⁴ As can be seen from the figures, perfluorocarbons are much denser than hydrocarbons but are also much more expansible and compressible. The results for the PFAAs globally show that these substances have densities, compressibilities, and expansivities between those of the *n*-alkanes and *n*-perfluoroalkanes. It can also be seen that,

when comparing substances with the same chain length, the properties of PFAAs lie closer to the corresponding *n*-perfluoroalkanes than to the *n*-alkanes.

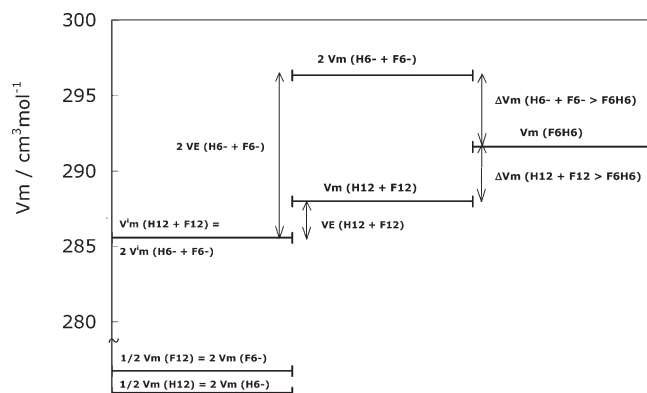
6. DISCUSSION

A global view of the results at 298.15 K and atmospheric pressure is presented in Figure 5, from which a number of interesting conclusions can be drawn. In the figure, the molar volumes of all studied PFAAs and *n*-perfluoroalkanes are plotted as a function of the total number of carbon atoms in the chain. Molar volumes of *n*-alkanes from the literature are also included for comparison. As can be seen from the figure, for the *n*-alkanes and *n*-perfluoroalkanes straight lines are obtained, the slope of which can be identified with the molar volume of the CH₂ and CF₂ groups, respectively, as 15.976 and 23.325 cm³ mol⁻¹. More interestingly, the molar volumes for the series (F4H5, F4H6, F4H8) also fall on a straight line. In this series, the length of the fluorinated segment is kept constant, while that of the hydrogenated segment is increased, thus the slope can be identified with the molar volume of the CH₂ group when bonded to a perfluorobutyl segment ($V_m(\text{CH}_2)_{\text{F}_4}$). As expected, the value obtained, $V_m(\text{CH}_2)_{\text{F}_4} = 16.444$ cm³ mol⁻¹, is 2.9% larger than the molar volume of the CH₂ groups in *n*-alkanes, previously mentioned. Similar reasoning can be applied to the series (F6H6, F6H8), (F4H6, F6H6), and (F4H8, F6H8) yielding, respectively, $V_m(\text{CH}_2)_{\text{F}_6} = 16.605$ cm³ mol⁻¹, $V_m(\text{CF}_2)_{\text{H}_6} = 24.87$ cm³ mol⁻¹, and $V_m(\text{CF}_2)_{\text{H}_8} = 25.018$ cm³ mol⁻¹. The results show that, when inserted in a PFAA molecule, the molar volumes of both CH₂ and CF₂ groups are larger than their usual value in *n*-alkanes and *n*-perfluoroalkanes and increase with the length of the hetero segment. The data are collected in Table 5.

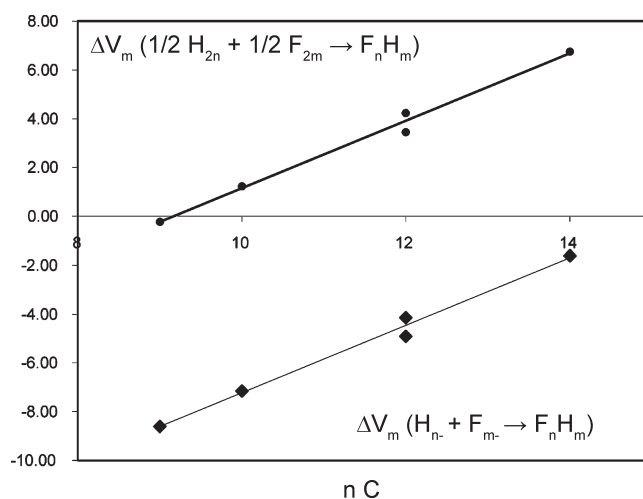
An attempt was made to interpret the results, by decomposing the molar volumes of the studied PFAAs into the molar volumes of the constituent segments, plus a volume change contribution resulting from mixing the hydrogenated and fluorinated segments and a specific term resulting from the formation of the alkyl–perfluoroalkyl bond. The molar volumes of the alkyl and perfluoroalkyl segments at 298.15 K can be obtained from

Table 5. Values of the Increment in V_m for CH_2 and CF_2 for the Three Studied Families of Compounds

	$V_m(\text{CH}_2)/$ $\text{cm}^3 \cdot \text{mol}^{-1}$	$V_m(\text{CF}_2)/$ $\text{cm}^3 \cdot \text{mol}^{-1}$	
<i>n</i> -alkanes	15.976	-	
constant F4 segment	16.444	2.9%	
constant F6 segment	16.605	3.9%	
perfluoroalkanes		23.325	
constant H6 segment		24.870	6.6%
constant H8 segment		25.018	7.3%

**Figure 6.** Scheme to obtain the contribution of the CH_2 – CF_2 junction to the molar volume of F_6H_6 .

literature data for the *n*-alkanes⁵⁵ (molar volumes as a function of the chain length) and for the perfluoroalkanes from our own experimental data. The volume change resulting from mixing hydrogenated and fluorinated segments can be obtained from the excess volume data for several mixtures of *n*-alkanes and perfluoroalkanes at 298.15 K from Lepori et al.²¹ Finally, the contribution resulting from the existence of the alkyl–perfluoroalkyl bond can be obtained by subtracting the previous two terms from the experimental molar volume. The bonding term should include contributions from several effects, namely, the presence of the dipole at the CH_2 – CF_2 junction, geometrical considerations (the cross-sectional diameter of the hydrogenated and fluorinated chains is highly incompatible relative to a close-packed arrangement. This fact contributes by itself to phase segregation. Bonding the two types of segments together will thus produce volume changes as a result of geometrical constrictions), and the reorganization of the liquid, reflecting the balance of the affinity/antipathy between the two types of segments, i.e., the building up of amphiphilic character. This procedure is illustrated in Figure 6 for F_6H_6 . The figure clearly shows how the molar volumes for the hexyl (H_6 -) and perfluorohexyl (F_6 -) segments (which are equivalent to half the molar volumes of *n*-dodecane and perfluorododecane, respectively) add to obtain the volume of 2 mol of an ideal mixture of these segments (equivalent to the molar volume of an ideal mixture of (*n*-dodecane + perfluorododecane), $V_m(\text{H}_{12} + \text{F}_{12})$). Also shown are the estimated excess volumes when mixing H_6 - and F_6 -segments or *n*-dodecane and perfluorododecane. As can be seen, these are not similar, as the excess volume depends on chain length. Finally, it is also clear that the molar volume of

**Figure 7.** Contribution of the CH_2 – CF_2 junction to the molar volume of PFAA as a function of total number of carbon atoms.

F_6H_6 lies between $V_m(\text{H}_6 + \text{F}_6)$ and $V_m(\text{H}_{12} + \text{F}_{12})$, although closer to the latter. This indicates that if a mixture of *n*-dodecane and perfluorododecane could be transformed into F_6H_6 by interchanging segments an increase in volume would occur. Alternatively, in a hypothetical mixture of F_6 - and H_6 - in which the segments were bonded together to form F_6H_6 , the volume would decrease.

Similar calculations were performed for all PFAAs, and the results are presented in Figure 7. As can be seen from the figure, in all cases the molar volumes of the PFAA are smaller than those of the corresponding mixtures of segments; i.e., the volume of the mixture would decrease on bonding the segments together. On the other hand, the molar volumes of four of the studied PFAAs are larger than those of the corresponding mixture of alkanes and perfluoroalkanes; i.e., an increase of the molar volume would occur on interchanging segments. The molar volume of F_4H_5 , however, is slightly smaller than that of an equimolar mixture of *n*-decane and perfluorooctane; that is, a volume contraction would occur in this case, either by bonding together the constituent segments or by interchanging segments between the parent molecules. Furthermore, in either case, the differences found contain the volume contribution of the CH_2 – CF_2 bond. As can be seen, these are not constant but increase with the total chain length of the PFAA molecules in a similar way, reflecting that they are different ways of expressing the same physical feature.

The results obtained for the PFAAs studied have been interpreted using two theoretical approaches: molecular dynamics simulations and the SAFT-VR equation of state.

Liquid densities were obtained from molecular dynamics simulations for F_4H_5 , F_4H_6 , and F_4H_8 as a function of temperature and pressure and as a function of temperature only, for F_6H_6 and F_6H_8 . Liquid densities were also calculated for F_5H_5 and found to be in excellent agreement with the simulations of Pierce et al.⁵⁶ The results are presented in Table 6 and plotted in Figure 8, from which a number of conclusions can be drawn. As can be seen from the figure, the simulations are able to predict the liquid densities in excellent agreement with the experimental results. Globally, the deviations lie between -2.4 and 1.4% , which are well within those usually found for

Table 6. Simulation Results for the Liquid Density of PFAA, at Different Temperatures and Pressures and Comparison with Experimental Results

density ($\text{kg}\cdot\text{m}^{-3}$)						
F4H5						
$p = 0.101325 \text{ MPa}$			$p = 25.33125 \text{ MPa}$			
T/K	simulation	experiment	dev. (%)	simulation	experiment	dev. (%)
278	1314 ± 6	1320.29	-0.5	1357 ± 5	1358.72	-0.1
298	1273 ± 4	1286.99	-1.1	1323 ± 3	1330.51	-0.6
313	1246 ± 7	1261.62	-1.3	1300 ± 4	1309.53	-0.7
333	1205 ± 6	1227.25	-1.8	1268 ± 4	1281.86	-1.1
353	1164 ± 7	1192.28	-2.4	1237 ± 6	1254.54	-1.4

$p = 50.66250 \text{ MPa}$			
T/K	simulation	experiment	dev. (%)
278	1386 ± 3	1388.99	-0.2
298	1359 ± 4	1363.70	-0.3
313	1338 ± 3	1345.08	-0.5
333	1310 ± 4	1320.75	-0.8
353	1284 ± 4	1296.90	-1.0

F4H6						
$p = 0.101325 \text{ MPa}$			$p = 25.33125 \text{ MPa}$			
T/K	simulation	experiment	dev. (%)	simulation	experiment	dev. (%)
278	1286 ± 5	1288.67	-0.2	1324 ± 5	1323.84	0.0
298	1252 ± 5	1257.75	-0.4	1294 ± 4	1297.39	-0.2
313	1224 ± 5	1234.27	-0.9	1272 ± 3	1277.73	-0.4
333	1187 ± 4	1202.59	-1.3	1243 ± 4	1251.82	-0.7
353	1149 ± 6	1170.46	-1.8	1213 ± 4	1226.23	-1.1

$p = 50.66250 \text{ MPa}$			
T/K	simulation	experiment	dev. (%)
278	1354 ± 3	1351.90	0.1
298	1326 ± 3	1328.08	-0.2
313	1306 ± 4	1310.56	-0.3
333	1280 ± 4	1287.65	-0.6
353	1256 ± 4	1265.19	-0.7

F4H8						
$p = 0.101325 \text{ MPa}$			$p = 25.33125 \text{ MPa}$			
T/K	simulation	experiment	dev. (%)	simulation	experiment	dev. (%)
278	1246 ± 4	1236.55	0.8	1284 ± 4	1267.06	1.4
298	1215 ± 5	1208.96	0.5	1251 ± 4	1243.10	0.6
313	1185 ± 4	1188.15	-0.2	1228 ± 4	1225.36	0.2
333	1155 ± 4	1160.24	-0.5	1200 ± 4	1202.03	-0.2
353	1120 ± 6	1132.22	-1.1	1170 ± 5	1179.04	-0.7

$p = 50.66250 \text{ MPa}$			
T/K	simulation	experiment	dev. (%)
278	1309 ± 4	1291.85	1.3
298	1280 ± 3	1270.14	0.8

Table 6. Continued

$p = 50.66250 \text{ MPa}$						
T/K	simulation	experiment	dev. (%)			
313	1256 ± 3	1254.20	0.2			
333	1232 ± 3	1233.40	-0.1			
353	1208 ± 4	1213.03	-0.4			

F6H6			F6H8			
$p = 0.101325 \text{ MPa}$			$p = 0.101325 \text{ MPa}$			
T/K	simulation	experiment	dev. (%)	simulation	experiment	dev. (%)
278	1427 ± 6	1418.32	0.6	1371 ± 4	1360.38	0.8
298	1387 ± 4	1386.33	0.0	1345 ± 5	1330.97	1.1
313	1357 ± 5	1362.15	-0.4	1314 ± 4	1308.93	0.4
333	1319 ± 7	1329.48	-0.8	1274 ± 5	1279.04	-0.4
353	1284 ± 5	1296.11	-0.9	1244 ± 4	1249.40	-0.4

pure *n*-alkanes and *n*-perfluoroalkanes. In most cases, the simulations predict densities slightly lower than the experimental, except for the heaviest PFAA at the lowest temperatures, but slightly overpredict the expansivity of all liquids. Moreover, for the three PFAAs studied in this work, the agreement between experimental and simulated densities improves at higher pressures.

It should be emphasized that the simulations were done using simple geometrical combining rules to obtain the cross interaction parameters. Song et al.¹⁷ have shown that for binary mixtures of *n*-alkanes + *n*-perfluoroalkanes the reduction of the F–H cross interaction by 25% changes significantly the enthalpy of mixing, bringing it close to the experimental results, but has little effect on the density, showing that this property is not very sensitive to small changes in the interactions. This behavior is also observed for the PFAAs studied, though to elucidate this point further it would be important to simulate other properties of PFAAs, namely, vapor pressures and vaporization enthalpies, and this will be done in future work.

Additionally, the F4H5, F4H6, and F4H8 liquids have been modeled with the hetero-SAFT-VR equation using a totally predictive approach. The number of spherical segments forming the alkyl and perfluoroalkyl chains was determined as in the previous paper of this series,²⁸ giving the values of 1.997, 2.332, 2.998, and 1.795 for pentyl, hexyl, octyl, and perfluorobutyl segments, respectively. The square-well parameters ϵ , σ , and λ for the alkyl and perfluoroalkyl chains and the binary interaction parameters that mediate the strength of the cross interaction ($\xi_{ij} = 0.840$ and $\gamma_{ij} = 1.0451$) were all taken from earlier work on the alkanes and perfluoroalkanes.^{57–59}

The results of the hetero-SAFT-VR predictions for the molar volume of all the PFAA compounds (the three studied here and the two studied in the previous work) at a pressure of 1 atm are presented in Figure 9, along with the corresponding experimental results. It can be seen that, although the expansivity is overpredicted by the theory, the error in the molar volumes compared to the experimental data is always less than 1%. This agreement is remarkable, especially considering that the theoretical results are true predictions, since no parameters were fitted to experimental data for the fluids being studied.

SAFT-VR calculations were also performed to predict the molar volumes of F4H5, F4H6, and F4H8 as a function of

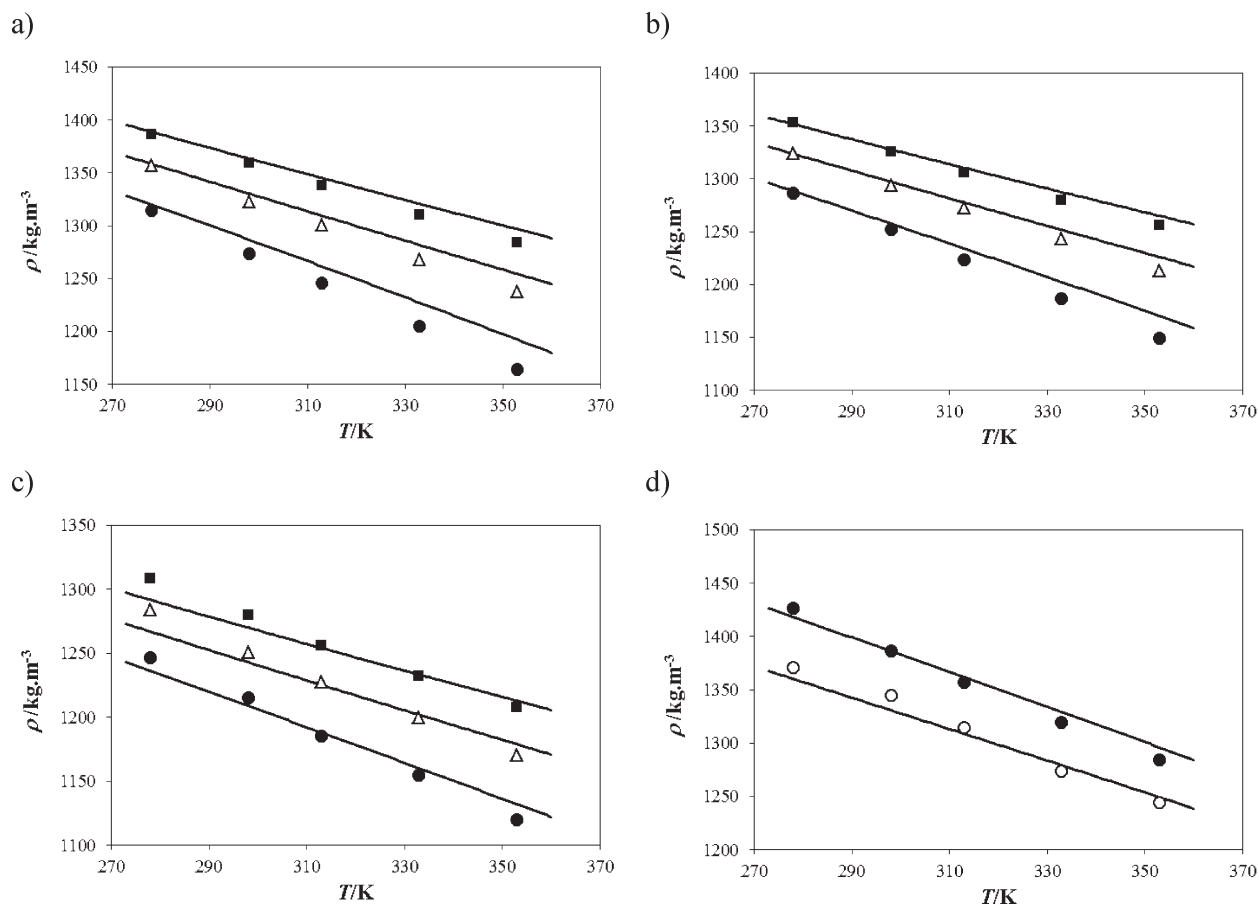


Figure 8. Comparison between experimental (lines) and simulated (points) densities as a function of temperature for: (a) F4H5 (●, 0.101325 MPa; △, 25.33125 MPa; ■, 50.6625 MPa); (b) F4H6 (idem); (c) F4H8 (idem); (d) ●, F6H6; ○, F6H8 at 0.101325 MPa.

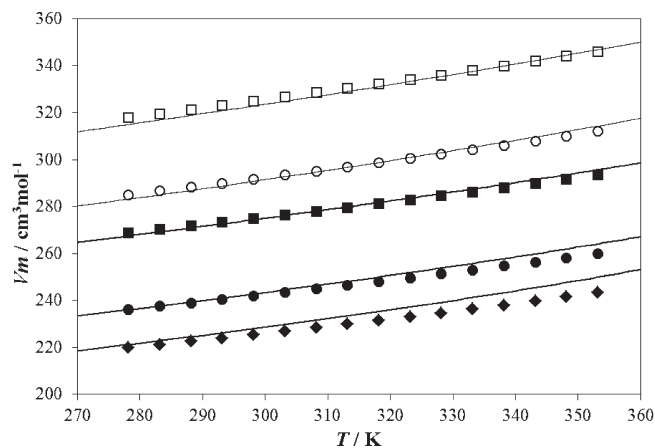


Figure 9. Comparison between experimental and SAFT-VR results of molar volume at atmospheric pressure as a function of temperature for five PFAAs. Experimental results: ◆, F4H5; ●, F4H6; ■, F4H8; ○, F6H6; □, F6H8. SAFT-VR predictions: lines.

pressure. The results for F4H8 are presented in Figure 10, along with the experimental data. From the figure, it can be seen that the theory overpredicts the compressibility since the slope of the theoretical curves is considerably larger than that of the experimental results; however, if a comparison is made directly between the predicted molar volumes and the experimental data, the error is

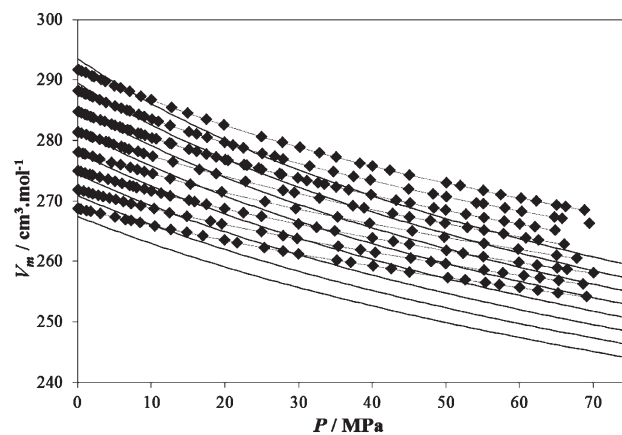


Figure 10. Comparison between experimental and SAFT-VR results of molar volume for F4H8 as a function of pressure at eight temperatures (from 278.15 to 348.15 K with intervals of 10 K). Points: experimental results. Lines: SAFT-VR predictions.

smaller than 3.5%, even at 600 bar. The results for the other PFAAs studied show similar behavior and so are not shown.

CONCLUSIONS

The liquid density of perfluorobutylpentane (F4H5), perfluorobutylhexane (F4H6), and perfluorobutyloctane (F4H8)

was measured as a function of temperature from 278.15 to 353.15 K and from atmospheric pressure to 70 MPa. The liquid density of *n*-perfluoropentane, *n*-perfluorohexane, *n*-perfluorooctane, and *n*-perfluorononane was also measured at room pressure, in the same temperature range. The results indicate that the molar volume of PFAAs is larger than that of mixtures of (*n*-alkanes + perfluoroalkanes) with similar chain length.

The results were further interpreted using the hetero-SAFT-VR equation of state. The perfluoroalkylalkanes were modeled as heterosegmented diblock chains, using parameters for the alkyl and perfluoroalkyl segments developed in earlier work. This fully predictive approach is able to estimate the liquid density of the perfluoroalkylalkanes at atmospheric pressure within 1% and at pressures up to 600 MPa within 3.5% without fitting to any experimental data for the PFAAs.

Finally, molecular dynamics simulations were performed using an atomistically detailed force field. The deviations between the simulated densities and experimental data lie between -2.4 and 1.4% for all the PFAAs studied and are comparable to those found for pure *n*-alkanes and *n*-perfluoroalkanes. In this case, the cross interaction parameters were taken as the geometric mean of the pure parameters; deviation from the geometric mean value was not needed to predict accurate PVT behavior. The ability of the OPLS all-atom force field to predict other physical properties of the PFAAs will be investigated in future work.

■ ASSOCIATED CONTENT

S Supporting Information. Supporting Tables 1–3. This material is available free of charge via the Internet at <http://pubs.acs.org>.

■ ACKNOWLEDGMENT

P.M. acknowledges funding from Fundação para a Ciência e Tecnologia, in the form of a PhD grant (No. SFRH/BD/39150/2007). E.J.M.F. acknowledges funding from the Fundação para a Ciência e Tecnologia through grant numbers POCI/QUI/61850/2004 and PEst-OE/QUI/UI0100/2011. C.M.C. and J.B.L. acknowledge support from the Office of Naval Research under grant numbers N00014-06-1-0624, N00014-09-1-0334, and N00014-09-1-0793 and gratefully acknowledge the National Energy Research Scientific Computing Centre, which is supported by the Office of Science of the Department of Energy under Contract No. DE-AC02-05CH11231, for computational resources. C.M.C. also acknowledges support from the Jacob Wallenberg Foundation and the National Science Foundation through grant numbers CTS-0829062 and CBET-1067642. L.F.G.M. acknowledges funding from Fundação para a Ciência e Tecnologia through grant POCTI/QUI/46299/2002. F.J.B. is grateful for financial support from project numbers FIS2010-14866 of the Spanish DGICYT (Dirección General de Investigación Científica y Técnica) and HP2005-045 of the Spanish MEC (Ministerio de Educación y Ciencia, Programa de Acciones Integradas), as well as for additional financial support from Universidad de Huelva and Junta de Andalucía.

■ REFERENCES

- (1) Krafft, M. P. *Adv. Drug Delivery Rev.* **2001**, *47*, 209.
- (2) May, G. *Chem. Br.* **1997**, *33*, 34.
- (3) Gross, U.; Papke, G.; Rudiger, S. *J. Fluorine Chem.* **1993**, *61*, 11.
- (4) Riess, J. G. *Chem. Rev.* **2001**, *101*, 2797.
- (5) Gladysz, J. A.; Curran, D. P. *Tetrahedron* **2002**, *58*, 3823.
- (6) Horvath, I. T.; Rabai, J. *Science* **1994**, *266*, 72.
- (7) Simons, J. H.; Dunlap, R. D. *J. Chem. Phys.* **1950**, *18*, 335.
- (8) Rowlinson, J. S.; Swinton, F. L. *Liquids and Liquid Mixtures*, 3rd ed.; Butterworth Scientific: London, 1982.
- (9) Siebert, E. M. D.; Knobler, C. M. *J. Phys. Chem.* **1971**, *75*, 3863.
- (10) Brode, S.; McDonald, I. R. *Mol. Phys.* **1988**, *65*, 1007.
- (11) Schoen, M.; Hoheisel, C. *Mol. Phys.* **1986**, *58*, 699.
- (12) Archer, A. L.; Amos, M. D.; Jackson, G.; McLure, I. A. *Int. J. Thermophys.* **1996**, *17*, 201.
- (13) Cui, S. T.; Cochran, H. D.; Cummings, P. T. *J. Phys. Chem. B* **1999**, *103*, 4485.
- (14) McCabe, C.; Galindo, A.; Gil-Villegas, A.; Jackson, G. *J. Phys. Chem. B* **1998**, *102*, 8060.
- (15) Duce, C.; Tinè, M. R.; Lepori, L.; Matteoli, E. *Fluid Phase Equilib.* **2002**, *199*, 197.
- (16) Schneider, G. M. *Fluid Phase Equilib.* **2002**, *199*, 307.
- (17) Song, W.; Rossky, P. J.; Maroncelli, M. *J. Chem. Phys.* **2003**, *119*, 9145.
- (18) Kirsch, P. *Modern Fluoroorganic Chemistry*; Wiley-VCH: Weinheim, 2004.
- (19) Morgado, P.; Tomás, R.; Zhao, H.; dos Ramos, M. C.; Blas, F. J.; McCabe, C.; Filipe, E. J. M. *J. Phys. Chem. C* **2007**, *111*, 15962.
- (20) Morgado, P.; Rodrigues, H.; Blas, F. J.; McCabe, C.; Filipe, E. J. M. *Fluid Phase Equilib.* **2011**, *306*, 76.
- (21) Lepori, L.; Matteoli, E.; Spanedda, A.; Duce, C.; Tinè, M. R. *Fluid Phase Equilib.* **2002**, *201*, 119.
- (22) Jang, S. S.; Blanco, M.; Goddard, W. A., III; Caldwell, G.; Ross, R. B. *Macromolecules* **2003**, *36*, 5331.
- (23) Turberg, M. P.; Brady, J. E. *J. Am. Chem. Soc.* **1988**, *110*, 7797.
- (24) Binks, B. P.; Fletcher, P. D. I.; Kotsev, S. N.; Thompson, R. L. *Langmuir* **1997**, *13*, 6669.
- (25) Mahler, W.; Guillon, D.; Skoulios, A. *Mol. Cryst. Liq. Cryst. Lett.* **1985**, *2*, 111.
- (26) Viney, C.; Russell, T. P.; Depero, L. E.; Twieg, R. J. *Mol. Cryst. Liq. Cryst.* **1989**, *168*, 63.
- (27) Viney, C.; Twieg, R. J.; Russell, T. P.; Depero, L. E. *Liq. Cryst.* **1989**, *5*, 1783.
- (28) Morgado, P.; Zhao, H.; Blas, F. J.; McCabe, C.; Rebelo, L. P. N.; Filipe, E. J. M. *J. Phys. Chem. B* **2007**, *111*, 2856.
- (29) Peng, Y.; Zhao, H.; McCabe, C. *Mol. Phys.* **2006**, *104*, 571.
- (30) dos Ramos, M. C.; Blas, F. J. *Mol. Phys.* **2007**, *105*, 1319.
- (31) Peng, Y.; Goff, K. D.; dos Ramos, M. C.; McCabe, C. *Fluid Phase Equilib.* **2009**, *277*, 131.
- (32) Wagner, W.; Prueß, A. *J. Phys. Chem. Ref. Data* **2002**, *31*, 387.
- (33) Cibulka, I.; Takagi, T. *J. Chem. Eng. Data* **1999**, *44*, 411.
- (34) Cibulka, I.; Takagi, T.; Růžicka, K. *J. Chem. Eng. Data* **2001**, *46*, 2.
- (35) McCabe, C.; Galindo, A.; Gil-Villegas, A.; Jackson, G. *Int. J. Thermophys.* **1998**, *19*, 1511.
- (36) McCabe, C.; Gil-Villegas, A.; Jackson, G. *J. Phys. Chem. B* **1998**, *102*, 4183.
- (37) dos Ramos, M. C.; Blas, F. J. *Mol. Phys.* **2010**, *108*, 1349.
- (38) Peng, Y.; Goff, K. D.; dos Ramos, M. C.; McCabe, C. *Ind. Eng. Chem.* **2010**, *49*, 1378.
- (39) dos Ramos, M. C.; McCabe, C. *Fluid Phase Equilib.* **2011**, *302*, 161.
- (40) dos Ramos, M. C.; Haley, J. D.; Westwood, J. R.; McCabe, C. *Fluid Phase Equilib.* **2011**, *306*, 97.
- (41) McCabe, C.; Gil-Villegas, A.; Jackson, G.; Del Rio, F. *Mol. Phys.* **1999**, *97*, 551.
- (42) Leonard, P. J.; Henderson, D.; Barker, J. A. *Trans. Faraday Soc.* **1970**, *66*, 2439.
- (43) Boublik, T. *J. Chem. Phys.* **1970**, *53*, 471.
- (44) Mansoori, G. A.; Carnahan, N. F.; Starling, K. E.; Leland, T. W. *J. Chem. Phys.* **1971**, *54*, 1523.
- (45) Gil-Villegas, A.; Galindo, A.; Whitehead, P. J.; Mills, S. J.; Jackson, G.; Burgess, A. N. *J. Chem. Phys.* **1997**, *106*, 4168.

- (46) Jorgensen, W. L.; Maxwell, D. S.; Tirado Rives, J. J. *Am. Chem. Soc.* **1996**, *118*, 11225.
- (47) Watkins, E. K.; Jorgensen, W. L. *J. Phys. Chem. A* **2001**, *105*, 4118.
- (48) Pádua, A. A. H. *J. Phys. Chem. A* **2002**, *106*, 10116.
- (49) Plimpton, S. J. *Comput. Phys.* **1995**, *117*, 1.
- (50) Allen, M. P.; Tildesley, D. J. *Computer Simulation of Liquids*; Oxford University Press: Oxford, 1987.
- (51) Haszeldine, R. N.; Smith, F. J. *Chem. Soc.* **1951**, 603.
- (52) Stiles, V. E.; Cady, G. H. *J. Am. Chem. Soc.* **1952**, *74*, 3771.
- (53) Piñeiro, M. M.; Bessières, D.; Gacio, J. M.; Saint-Guirons, H.; Legido, J. L. *Fluid Phase Equilib.* **2004**, *220*, 127.
- (54) Cibulka, I.; Hnědkovský, L. *J. Chem. Eng. Data* **1996**, *41*, 657.
- (55) Cibulka, I. *Fluid Phase Equilib.* **1993**, *89*, 1.
- (56) Pierce, F.; Tsige, M.; Borodin, O.; Perahia, D.; Grest, G. S. *J. Chem. Phys.* **2008**, *128*, 214903.
- (57) McCabe, C.; Jackson, G. *Phys. Chem. Chem. Phys.* **1999**, *1*, 2057.
- (58) Bonifácio, R. P.; Filipe, E. J. M.; McCabe, C.; Gomes, M. F. C.; Pádua, A. A. H. *Mol. Phys.* **2002**, *100*, 2547.
- (59) Morgado, P.; McCabe, C.; Filipe, E. J. M. *Fluid Phase Equilib.* **2005**, *228*, 389.
- (60) Burger, L. L.; Cady, G. H. *J. Am. Chem. Soc.* **1951**, *73*, 4243.
- (61) Dias, A. M. A.; Gonçalves, C. M. B.; Caço, A. I.; Santos, L. M. N. B. F.; Piñeiro, M. M.; Vega, L. F.; Coutinho, J. A. P.; Marrucho, I. M. *J. Chem. Eng. Data* **2005**, *50*, 1328.
- (62) Dunlap, R. D.; Murphy, C. J.; Bedford, R. G. *J. Am. Chem. Soc.* **1958**, *80*, 83.
- (63) Kennan, R. P.; Pollack, G. L. *J. Chem. Phys.* **1988**, *89*, 517.
- (64) Dias, A. M. A.; Caço, A. I.; Coutinho, J. A. P.; Santos, L. M. N. B. F.; Piñeiro, M. M.; Vega, L. F.; Costa Gomes, M. F.; Marrucho, I. M. *Fluid Phase Equilib.* **2004**, *225*, 39.
- (65) Mustafaev, M. R.; Naziev, Y. M.; Kagramanov, M. K. *High Temp.* **1995**, *33*, 359.